HHS Public Access

Author manuscript

Nat Cell Biol. Author manuscript; available in PMC 2016 May 01.

Published in final edited form as:

Nat Cell Biol. 2015 November ; 17(11): 1504–1511. doi:10.1038/ncb3252.

High Speed Depolymerization at Actin Filament Ends Jointly Catalyzed by Twinfilin and Srv2/CAP

Adam B. Johnston[1], **Agnieszka Collins**[1], and **Bruce L. Goode**[1]

1

Abstract

Purified actin filaments depolymerize slowly, and cytosolic conditions strongly favor actin assembly over disassembly, which has left our understanding of how actin filaments are rapidly turned over in vivo incomplete [1,2]. One mechanism for driving filament disassembly is severing by factors such as Cofilin. However, even after severing, pointed end depolymerization remains slow and unable to fully account for observed rates of actin filament turnover in vivo. Here we describe a mechanism by which Twinfilin and Cyclase-associated protein work in concert to accelerate depolymerization of actin filaments by 3-fold and 17-fold at their barbed and pointed ends, respectively. This mechanism occurs even under assembly conditions, allowing reconstitution and direct visualization of individual filaments undergoing tunable, accelerated treadmilling. Further, we use specific mutations to demonstrate that this activity is critical for Twinfilin function in vivo. These findings fill a major gap in our knowledge of mechanisms, and suggest that depolymerization and severing may be deployed separately or together to control the dynamics and architecture of distinct actin networks.

Many cellular processes depend on the rapid remodeling and turnover of actin networks [1,2]. However, purified actin filaments disassemble very slowly, limited by a slow rate of ADP-actin subunit dissociation from pointed ends: 0.16–0.27 s^{-1} [3,4]. These turnover rates are at least 100-fold slower than reported rates of filament turnover in vivo [5,6], suggesting that cells have mechanisms that promote the rapid disassembly of actin filaments. One mechanism is through Cofilin-mediated severing [7], aided by factors such as Aip1 and Coronin [8]. Here, we describe a distinct and complementary mechanism, wherein Twinfilin and Srv2/CAP (Cyclase-associated protein) [9,10] work together to greatly accelerate shortening of filaments at their barbed and pointed ends.

Twinfilin is a member of the ADF/Cofilin-homology (ADF-H) domain family and consists of two ADF-H domains, a ‘linker’ sequence, and a short ‘tail’ [9,11] (Fig. 1A). Twinfilin localizes to many different actin structures in vivo, including yeast cortical actin patches, Drosophila bristles, and mammalian lamellipodia, cell-cell contacts, filopodial tips, and

Correspondence and requests for materials should be addressed to B.L.G. (goode@brandeis.edu).

Author Contributions: A.B.J. and B.L.G. designed experiments. A.C. performed electron microscopy experiments. A.B.J. performed all other experiments and analyses. A.B.J. and B.L.G. wrote the paper.

The authors declare no competing financial interests.

stereocilia tips [11–17]. Genetic interactions between Twinfilin and Cofilin in yeast and flies have long suggested a role in actin disassembly [11,13], yet the primary activities described for Twinfilin have been actin monomer sequestering [11–13] and suppression of barbed end growth [18,19]. Therefore, we investigated the potential role of Twinfilin in promoting actin disassembly.

In bulk assays, we tested the effects of 1 μM yeast Twinfilin (Twf1), which is its estimated cellular concentration in yeast (Fig 1B; and [20]). Twf1 had no effect on the rate of pointed end actin filament disassembly either alone (Fig. 1C, purple curve) or in the presence of Cofilin (Supplemental Fig. 1A). Given its structural homology with Cofilin [19,21], we considered whether Twf1 might work with Srv2/CAP, which enhances Cofilin-mediated severing [22,23]. Indeed, in the combined presence of Twf1 and Srv2 (full-length), we observed concentration-dependent stimulation of filament disassembly (Fig. 1C,D). The ability of Srv2 to enhance Cofilin-mediated severing depends on its N-terminal half (N-Srv2) (Fig. 1A), consisting of an oligomerization domain (OD) and a helical folded domain (HFD) that binds F-actin and Cofilin [22–24]. N-Srv2 was sufficient to stimulate actin disassembly with Twf1 (Fig. 1E), and a mutation in the HFD (*srv2-91*) that disrupts enhancement of Cofilin-mediated severing also abolished Twf1-mediated disassembly, as did Srv2ΔOD, which disrupts formation of Srv2 hexameric *shuriken* structures [23,25]. Importantly, mouse homologs of Srv2 (mCAP1) and Twinfilin (mTwf1) also stimulated actin disassembly (Fig. 1F), demonstrating functional conservation across distant species.

Next, we directly visualized the effects of Twf1 and Srv2 on individual actin filaments using total internal reflection fluorescence (TIRF) microscopy. Filaments were polymerized to a sufficient length (> 10 μm) and sparsely tethered by incorporation of a low percentage of biotin-actin. Then, the actin monomer-containing solution was flowed out and replaced with proteins of interest (with no actin monomers present). Barbed ends were identified by their faster polymerization kinetics prior to flow-in, enabling us to follow and separately measure effects at each end of the filament. In control reactions, filaments depolymerized at rates of 0.34 subunits s^{-1} at pointed ends, and 1.46 subunits s^{-1} at barbed ends (Fig. 1G,H), similar to reported rates [4]. Flowing in Cofilin (Cof1) led to severing all along the lengths of filaments. In contrast, flowing in Twf1 and N-Srv2 induced rapid depolymerization of filaments from their ends, with no visible severing (Fig. 1G, Supplemental Video 1). Filaments shortened from their pointed ends at 5.68 subunits s^{-1}, and at their barbed ends at 4.17 subunits s^{-1} (Fig. 1H). Thus, Twf1 and N-Srv2 accelerated depolymerization ~17-fold at pointed ends and ~3-fold at barbed ends compared to control reactions.

Capping Protein restricted filament shortening to pointed ends (Fig. 1I, Supplemental Video 2). In the absence of Capping Protein, Twf1 alone induced barbed end shortening at rates similar to Twf1 and N-Srv2, but had no effect on pointed ends. Thus, Twf1 is sufficient to accelerate barbed end shortening, whereas Twf1 and N-Srv2, or full length Srv2 (Supplemental Fig. 1B), are together required for accelerated pointed end shortening. Twf1 and N-Srv2 could accelerate the disassembly of ADP- but not ADP+P_i-F-actin, indicating that this activity is controlled by the nucleotide state of F-actin, as for Cofilin severing [26] (Fig. 2A, Supplemental Fig. 1C,D). Further, depolymerization was unaffected by the actin monomer sequestering protein Vitamin-D Binding Protein (VDBP) (Fig. 1H), suggesting

that the effects of Twf1 on depolymerization are unrelated to its monomer sequestering function.

Cellular conditions strongly favor assembly over disassembly, as the cytosol contains a concentration of ATP-actin monomers orders of magnitude above the critical concentration for actin assembly [2]. Thus, a longstanding question has been how cells induce rapid disassembly of filaments under assembly-promoting conditions. To address this, we polymerized DY647-actin (magenta, Fig. 2B,C), then flowed in 1 μM OG-actin monomers (cyan) and 5 μM Profilin (an actin monomer-binding protein that restricts growth to barbed ends), with or without Twf1 and N-Srv2. In reactions lacking Twf1 and N-Srv2, filaments elongated at their barbed ends (cyan) while the pre-assembled regions (magenta) persisted. In reactions containing Twf1 and N-Srv2 (each at 0.5 or 1 μM), filaments polymerized at their barbed ends concurrent with rapid depolymerization at their pointed ends (Fig. 2C, Supplemental Video 3). These effects were not observed in reactions containing either Twf1 or N-Srv2 alone (Fig. 2B). Thus, the Twf1-Srv2 activity has enabled us to reconstitute and directly observe non-steady state treadmilling of individual actin filaments.

We next varied conditions to tune the rate of treadmilling. Increasing the concentration of Twf1 and N-Srv2 while maintaining a fixed concentration of G-actin resulted in faster rates of pointed end depolymerization, but abrogated barbed end growth (Fig. 2D). Higher concentrations of Twf1 and N-Srv2 completely suppressed growth, and actually induced barbed end depolymerization. However, elevating the concentration of G-actin restored barbed end growth while still maintaining depolymerization effects at the pointed ends (Fig. 2E). Thus, we were able to separately tune the dynamics at each end of the filament. Further, a close examination of individual filaments under conditions that support a near-zero net barbed end growth rate revealed alternating runs of polymerization and depolymerization (Fig. 2F, Supplemental Video 4). This was evident from the repeated appearance, and subsequent loss, of a small region of cyan-labeled polymer at the barbed end of an otherwise magenta filament. These observations suggest that processive associations of Twf1 and/or N-Srv2 at the barbed end underlies depolymerization runs, during which time growth at the barbed end is also blocked. Such activity could underlie the reported effects of mouse Twinfilin blocking barbed end growth in bulk assays [18,19].

We also asked whether the Twf1-Srv2 depolymerization mechanism could work in concert with Cofilin-mediated severing, and observed that together they more rapidly disassemble filaments than either mechanism alone (Fig. 3A, Supplemental Fig. 2A, Supplementary Video 5). In these reactions, severing produced short fragments that were subsequently depolymerized rapidly from their pointed ends (Supplemental Video 6). These observations demonstrate that the two mechanisms are complementary, consistent with genetic interactions between Twinfilin and Cofilin [11,13].

The TIRF assays in which Twf1 and N-Srv2 accelerate depolymerization contain no monomeric actin (e.g., Fig. 1G–I), suggesting that one or both proteins directly interact with F-actin to enhance depolymerization. N-Srv2 binds F-actin [24], and we found that Twf1 also binds F-actin in a concentration-dependent manner (Fig. 3B). However, it was not possible to reach saturated F-actin binding in these assays because Twf1 also shifts actin to the

supernatant fraction due to its monomer sequestering activity. Interestingly, F-actin binding was previously observed for *Drosophila* and mouse Twinfilin [13,19], but may not have received attention because of the higher affinity of Twinfilin for G-actin.

Further analysis showed that at least three distinct domains in Twf1 are required for accelerated pointed end depolymerization, including its two ADFH domains and its C-terminal tail (Fig. 3C, Supplemental Fig. 2B,C). The C-terminal tail was sufficient to bind F-actin and contributed to the F-actin binding affinity of full-length Twf1 (Fig. 3B,D). Further, Twf1-10 tail (305-322) alone was sufficient to bind F-actin, albeit with reduced affinity compared to intact tail (Fig 3D), possibly explaining why Twf1-10 showed robust depolymerization activity (Supplemental Fig. 2B,D), whereas Twf1Δtail (1-304) lacked any activity. These observations show that accelerated depolymerization requires multiple actin-binding domains in Twf1, including a previously unrecognized actin-binding site in its tail region.

Electron microscopy analysis revealed that Twf1 alters the structure of actin filaments. Control filaments were long, smooth and straight. Decoration by Twf1 caused filaments to become highly ‘kinked’ or supercoiled (Fig. 3E,F, Supplemental Fig. 3), with an appearance distinct from the ‘twist’ induced by Cofilin [27] (Supplemental Fig. 3). In samples containing N-Srv2, we could clearly see hexameric complexes on filament sides (Fig. 3E), and filaments took on a ragged appearance (Supplemental Fig. 3), as described [24]. It was not possible to image filaments in the combined presence of N-Srv2 and Twf1, because even a brief incubation with the two proteins caused filaments to become extremely fragile and break upon contact with the grid (Supplemental Fig. 3), and prolonged incubation resulted in complete disassembly.

To test the importance of Twf1-mediated depolymerization in vivo, we designed specific mutations in Twf1 that disrupt its activities with N-Srv2. Cof1-9 is a mutant with normal severing activity, but is insensitive to enhancement by N-Srv2 [23,25]. Therefore, we introduced analogous mutations into the N- and C-terminal ADFH domains of Twf1, individually and combined, to produce Twf1-9N, Twf1-9C, and Twf1-99 (Fig. 4A). In plasmid shuffle assays, *twf1-99* failed to rescue the synthetic lethality of *twf1*Δ *cof1-22*, and *twf1-9N* and *twf1-9C* alleles only partially rescued growth (Fig. 4B). These mutants were minimally impaired for actin monomer binding (Fig. 4C); in contrast, a control mutant (Twf1-3) that targets the actin-binding surfaces on both ADFH domains [20] displayed greatly reduced monomer affinity. Twf1-99 was severely defective in accelerating pointed end depolymerization with N-Srv2 (Fig. 4C). Although not anticipated, Twf1-99 was also defective in accelerating barbed end depolymerization both in the presence and absence of N-Srv2 (Fig 4D). These results demonstrate that Twf1 cellular function depends on its accelerated depolymerization activity; however, they do not allow us to distinguish between the importance of its depolymerization effects at barbed versus pointed ends.

To better understand the mechanism(s) underlying enhanced depolymerization, we varied the concentrations of Twf1 and N-Srv2. With 500 nM Twf1 and N-Srv2, the majority of filaments shortened rapidly at their barbed ends, while a few filaments shortened at a reduced rate comparable to control filaments (Fig. 5A). However, the pointed ends of the

exact same filaments shortened at a similar accelerated rate in every case (Fig. 5B). Rates of pointed end depolymerization also scaled with the concentration of Twf1 and N-Srv2 (tight clustering in the distribution of rates at each condition), whereas rates of barbed end depolymerization for the same filaments had a broader, almost bimodal distribution. These observations suggest that the accelerated depolymerization mechanism(s) may be distinct at barbed versus pointed ends, which is consistent with alternating runs of polymerization and depolymerization we observed at barbed ends in our treadmilling assays (Fig. 2F).

Using multi-wavelength single molecule TIRF microscopy, we directly observed SNAP-549-Twf1 (yellow) molecules (Supplemental Fig. 4A,B) interacting with both the sides and barbed ends of OG-actin filaments (magenta) in the presence and absence of N-Srv2 (Fig. 5C,D, Supplemental Fig. 4C,D). The average dwell time of SNAP-549-Twf1 molecules on barbed ends increased from 75 s in the absence of N-Srv2 to 592 s in the presence of N-Srv2, but the dwell time was not enhanced by N-Srv2-91 (Fig. 5E). Barbed end association of SNAP-549-Twf1 persisted while filaments were depolymerizing, suggesting a processive attachment (Fig. 5D, Supplemental Video S). The increased dwell time of Twf1 at barbed ends in the presence of N-Srv2 suggested the involvement of direct Twf1-Srv2 interactions, which have been reported [28,29]. In supernatant depletion assays, GST-N-Srv2 depleted soluble Twf1 specifically in the presence of G-actin (Fig. 5F, Supplemental Fig. 5A), similar to reported Cof1-N-Srv2 interactions [25]. However, by electron microscopy we were able to visualize complexes formed by Twf1 and N-Srv2 even in the absence of G-actin. When incubated with Twf1, the regularly shaped hexameric N-Srv2 structures gained 3–4 long protrusions, often with a ‘beaded’ appearance (Fig. 5G, Supplemental Fig. 5B,C). The presence of G-actin gave protrusions a shorter and more rounded appearance (Fig. 5G, Supplemental Fig. 5D). Together, these results suggest that Twf1 interacts directly with N-Srv2, possibly facilitated by G-actin, to form a structure that more persistently associates with barbed ends during depolymerization compared to Twf1 alone.

The average dwell time of SNAP-549-Twf1 molecules on the sides of filaments was not significantly affected by N-Srv2 (Fig. 5E). Further, SNAP-549-Twf1 was rarely seen at filament pointed ends. Together with our ultrastructural data (Fig. 3E,F), these findings support a model in which Twf1 and N-Srv2 accelerate pointed end depolymerization through their combined and possibly independent interactions with filament sides and conformational effects on F-actin [24].

In sum, our findings identify the long sought-after actin end-depolymerase. Although Twinfilin and Cofilin are members of the same ADF-H domain superfamily [9], they clearly have mechanistically distinct roles in promoting actin disassembly. Further, our data show that when severing is partially impaired in vivo, the depolymerization activity of Twf1 becomes vital. Enhanced severing by Cofilin, Aip1, and Coronin produces capped F-actin fragments ~20 subunits long [8,30], but these fragments will require over a minute to depolymerize based on a 0.27 subunits s^{-1} dissociation rate at pointed ends [3]. Twf1 and Srv2 can increase the depolymerization rate by 17-fold, such that the same fragments would depolymerize in 4–5 seconds. Therefore, mechanisms of enhanced severing combined with accelerated depolymerization together would yield extremely high rates of actin turnover,

such as those observed at the leading edge [5]. In addition, the depolymerization mechanisms we have described may play an important role in controlling the length and turnover of actin arrays comprised of longer filaments, such as filopodia and stereocilia, where Twinfilin localizes [12,16,17].

Methods

Plasmids

Expression plasmids pGAT2-Twf1 (1-332) and pGAT2-Twf1-10 (1-322) have been described [11,31]. We generated pGAT2-Twf1Δtail (1-304), pGAT2-Twf1 N (1-135), pGAT2-Twf1 C (165-304), and pGAT2-Twf1 CT (165-332) by PCR amplifying the indicated regions of Twf1 and subcloning into the XhoI and HindIII sites of pGAT2. To generate MBP-tagged Twf1 tail (305-332) and Twf1-10 tail (305-322), we annealed complementary primers encoding the tail regions and ligated this into the EcoRI and HindIII sites of pMAL-C2. The SNAP-Twf1 expression plasmid was generated by PCR amplifying the intact Twf1 coding region and subcloning it into the BamHI and NotI sites of pGEX-6p-1-SNAP. pGAT2-Twf1-1 (RR 88,90 AA), pGAT2-Twf1-2 (KR 254, 256 AA), pGAT2-Twf1-3 (RR 88,90 AA, KR 254,256 AA), pGAT2-Twf1-9N (DSTS 36-39 AAAA), pGAT2-Twf1-9C (DE 203,207 AA), and pGAT2-Twf1-99 (DSTS 36-39 AAAA, DE 203,207 AA) were generated by site directed mutagenesis of pGAT2-Twf1. pHAT2-FL-Srv2 (1-526), pHAT2-N-Srv2 (1-259), pHAT2-C-Srv2 (253-526), and pHAT2-Srv2ΔOD (51-526) have been described [25,32,33]. pHAT2-Srv2-91 and pHAT2-N-Srv2-91 (RILKE 102-106 AIAAA) were generated by site-directed mutagenesis of pHAT2-FL-Srv2 and pHAT2-N-Srv2, respectively. Plasmids for expressing GST-N-Srv2 [32], yeast Cofilin [34], yeast Capping Protein [34], and human Profilin [34] have been described.

Protein Expression and Purification

Rabbit skeletal muscle actin [35], biotinylated actin [36], pyrenyliodoacetamide-labeled actin (pyrene actin) [37], and Oregon-Green-labeled actin [4] were purified as described. DY647-actin was purified as per Oregon-Green-labeled actin, but using DY647-P1 maleimide dye (Dyomics, Jena, Germany). Yeast Cofilin [34], yeast Capping Protein [34], and human Profilin [34] were purified as described.

Twf1 polypeptides (full-length, fragments, and point mutants) were expressed as glutathione-S-transferase (GST) fusion proteins in *E. coli* strain BL21 (DE3). Cells were grown to log phase at 37°C, then expression was induced for 16 h at 18°C by addition of 0.4 mM isopropyl-β-D-thiogalactopyranoside (IPTG). Cells were harvested by centrifugation, washed with 25 mL water, and resuspended in 15 mL of PBS supplemented freshly with 0.5 mM dithiothreitol (DTT), 1 mM phenylmethylsulphonyl fluoride (PMSF), and a standard mixture of protease inhibitors. Cells were lysed by incubation with lysozyme (0.5 mg/mL) on ice for 15 min followed by sonication. The cell lysate was clarified by centrifugation at 14,000 g for 15 min and incubated at 4°C (rotating) for at least 2 h with 0.5 mL glutathione-agarose beads (Sigma-Aldrich, St. Louis, MO). Beads were washed 5 times in PBS, and then Twinfilin was cleaved from GST by incubation with thrombin (5 U/mL; Sigma-Aldrich) for 4 h at room temperature. Beads were pelleted, and the supernatant was concentrated to ~0.3

mL in an Amicon Ultra centrifugal filter device (Millipore, Bedford, MA), then further purified by size exclusion chromatography on a Superdex75 column (GE Healthcare, Pittsburgh, PA) equilibrated in TK buffer (10 mM Tris-HCl pH 7.5, 50 mM KCl, 0.5 mM DTT). Peak fractions were pooled, concentrated in an Amicon Ultra centrifugal filter device, aliquoted, snap-frozen in liquid N_2, and stored at −80°C.

Wild type and mutant His6-tagged yeast full-length (FL)-Srv2, Srv2 fragments, and N-Srv2-91 were expressed in *E. coli* BL21 (pRARE) cells and harvested as described above for Twf1. Cells were lysed by sonication in 20 mM phosphate buffer pH 7.4, 300 mM NaCl, 1 mM DTT (lysis buffer) supplemented with 10 mM imidazole and a standard mixture of protease inhibitors. Clarified lysates were incubated with Ni^{2+}-NTA beads (Qiagen, Valencia, CA) for 2 hr at 4°C and then transferred to a poly-prep chromatography column (Bio-Rad, Hercules, CA). The resin was washed with 10 column volumes of lysis buffer supplemented with 50 mM imidazole. Proteins were eluted with 5 column volumes of lysis buffer supplemented with 250 mM imidazole, concentrated, and purified further on a Superose 6 gel filtration column (GE Healthcare) equilibrated in TK buffer. Peak fractions were pooled, concentrated in an Amicon Ultra centrifugal filter device, aliquoted, snap-frozen in liquid N_2, and stored at −80°C.

MBP-tagged Twf1 tail (305-332) and Twf1-10 tail (305-322) were expressed as above, then the cell lysate was clarified by centrifugation at 14,000 g for 15 min and incubated for 2 h at 4°C (rotating) with 0.5 mL amylose resin (NEB, Ipswich, MA). The resin was washed with 10 column volumes of PBS. Proteins were eluted with 1 mL of MBP elution buffer (10 mM Tris-HCl pH 7.5, 10 mM maltose, 50 mM NaCl, 1 mM DTT, 1 mM PMSF, standard mix of protease inhibitors), concentrated, and purified further on a Superdex 75 gel filtration column (GE Healthcare) equilibrated in TK buffer. Peak fractions were pooled, concentrated in an Amicon Ultra centrifugal filter device, aliquoted, snap-frozen in liquid N_2, and stored at −80°C.

Cells expressing GST-tagged SNAP-Twf1 were lysed, and the cleared supernatant was bound to glutathione-agarose beads as described above for Twf1. Immobilized GST-SNAP-Twf1 was labeled for 2 h at room temperature with 25 μM SNAP-Surface 549 dye (NEB) or SNAP-Biotin 549 dye (NEB). Twf1 was then cleaved from GST by incubation with Prescission Protease for 1 h at room temperature, and further purified by gel filtration on a Superdex75 column in TK buffer, concentrated, and stored as described above. Concentration of SNAP-tagged protein and degree of labeling were determined by densitometry of Coomassie-stained bands on SDS-PAGE gels compared to BSA standards, and by measuring fluorophore absorbance in solution using the extinction coefficients: SNAP-549: ε560 = 140,300 M^{-1} cm^{-1}. Labeling efficiencies of 15.5% and 58% were achieved for SNAP-549-Twf1 and SNAP-549-biotin-Twf1, respectively. Concentration and degree of labeling of OG-actin were determined as described [4].

Bulk pyrene F-actin disassembly assays

At time zero, preassembled F-actin (2 μM final, 10% pyrene labeled) was mixed with the indicated proteins or control buffer, along with 3 μM vitamin-D-binding protein (VDBP)/human plasma Gc-globulin (Sigma-Aldrich). Fluorescence was monitored for 1000 s at

25°C at 365-nm excitation and 407-nm emission in a fluorescence spectrophotometer (Photon Technology International, Lawrenceville, NJ). All pyrene fluorescence curves are representative results from experiments repeated in at least 2–3 independent trials.

Total Internal Reflection Fluorescence (TIRF) Microscopy

In all experiments, 24x60 mm coverslips (Fisher Scientific, Pittsburgh, PA) were first cleaned by sonication in detergent for 60 min, followed by successive sonication in 1M KOH and 1M HCl for 20 min each, then sonication in ethanol for at least 60 min. Coverslips were then washed extensively with ddH_2O, dried in an N_2-stream, layered with 200 μl of 80% ethanol pH 2.0, 2 mg/mL methoxy-poly(ethylene glycol)-silane and 2 μg/mL biotin-poly(ethylene glycol)-silane (Laysan Bio Inc., Arab, AL), and incubated for 16 h at 70°C. Flow cells were assembled by rinsing PEG-coated coverslips extensively with ddH_2O, then attaching it to a flow chamber (Ibidi, Martinsried, Germany) with double-sided tape (2.5 cm x 2 mm x 120 μm) and five minute epoxy resin. Oregon Green (OG)-labeled actin was prepared as described [4], and DY647-labeled actin was prepared equivalently.

For flow-in experiments, flow cells were incubated for 2 min with HBSA (HEK buffer with 1% BSA) with 0.1 mg/mL Streptavidin. Flow cells were then equilibrated with 1x TIRF buffer (10 mM imidazole, 50 mM KCl, 1 mM $MgCl_2$, 1 mM EGTA, 0.2 mM ATP, 10 mM DTT, 15 mM glucose, 20 μg/mL catalase, 100 μg/mL glucose oxidase, and 0.5% methylcellulose (4000 cP), pH 7.4). Reactions were initiated by rapidly diluting actin monomers (1 μM final, 10% OG- or 5% DY647-labeled, 0.5 % biotinylated) into 1x TIRF buffer and transferring the mixture to a flow chamber. After a few minutes of actin polymerization, the reaction mixture was replaced with TIRF buffer lacking actin monomers, with or without Twf1 and/or Srv2 and/or Capping Protein.

For TIRF experiments performed under assembly-promoting conditions, the flow-in mixture also included actin monomers and/or Profilin. In experiments addressing the actin nucleotide preference of Cof1 or Twf1 and Srv2, 35 mM free P_i was included in the reactions. Based on rate constants for ATP hydrolysis and P_i release [38,39], pre-assembled filaments in reactions where P_i is not included should consist predominantly of ADP-bound actin subunits by the time of flow-in; however, inclusion of free P_i drives filaments into the ADP+P_i-bound state [26].

Flow-through was achieved using a syringe-pump (Harvard Apparatus, Holliston, MA). Time-lapse TIRF microscopy was performed using a Nikon-Ti200 inverted microscope equipped with a 150 mW Ar-Laser (Melles Griot, Carlsbad, CA), a TIRF-objective with a N.A. of 1.49 (Nikon Instruments Inc., New York, NY), and an EMCCD camera (Andor Ixon, Belfast, Northern Ireland). During measurements, optimal focus was maintained using the Perfect Focus System (Nikon Instruments Inc.). Images were captured every 5 s. The pixel size corresponded to 0.27 μm. Filament depolymerization rates were determined by tracing filaments in ImageJ (http://rsbweb.nih.gov/ij/) and measuring the change in length of individual filaments for 15–20 min after flow-in, or until filaments disappeared. Differences in fluorescence intensity along the length of the filament, or the boundary between OG- and DY647-labeled segments of filaments, were used as fiduciary markers to distinguish between barbed- and pointed-end depolymerization. Quantification of total filament levels in

TIRF reactions was carried out by first subtracting background and converting the image to binary pixels in ImageJ, then measuring total fluorescence intensity in the field of view over time. Curves shown in Figures 2A and 3A, and Supplemental Figure 1C, are averages of the measurements for two fields of view from the same reaction, with each field of view being about 25 times larger than the accompanying time-lapse images.

For single-molecule bleaching experiments, 0.1 nM SNAP-549-biotin-Twf1 in TIRF buffer without glucose oxidase and catalase was transferred into a flow cell as above, and immobile spots (anchored via Streptavidin to the biotin-PEG on the slide surface) were subjected to continuous illumination and imaged every 0.1 s. Fluorescence intensities of spots were obtained by measuring the integrated fluorescence signal from a small region of interest in ImageJ. Then, stepwise reductions in the integrated fluorescence intensity time records of individual spots were subjectively identified and counted. 75 spots in each of 2 independent reactions were measured.

For determination of protein oligomeric state by single molecule fluorescence, the measured distribution of fluorescence intensity or distribution of numbers of photobleaching steps was compared to the probability distribution p(*i*) of the number of fluorescent subunits *i* predicted for a protein oligomer consisting of n monomers, as calculated from the binomial distribution based on the measured subunit labeling stoichiometry s, as

$$p(i) = \left(\frac{n!}{i!(n-i)!}\right) s^i (1-s)^{n-i}$$

This approach is expected to be valid because SNAP-tagged protein monomers each have only a single site for reaction with the benzylguanine-dye adduct. Consistent with this, measured values of s were always <1.

Electron microscopy

Actin (20 μM) was polymerized for 1 h at 25°C, then diluted to 2 μM in F-buffer (50 mM KCl, 2 mM $MgCl_2$, 0.2 mM EGTA, 1 mM DTT, 5 mM Tris, pH.8) and incubated at 25°C for 3 min with Twf1, N-Srv2, or Twf1 and N-Srv2 (0.5 μM each). Samples were diluted two-fold in F-buffer and adsorbed to glow discharged formvar/carbon-coated 200 mesh copper grids for 15–20 s, blotted to remove excess solution, negatively stained with 1% (w/v) uranyl acetate for 1 min, blotted again, and allowed to air-dry. For imaging individual proteins in the absence of actin, 0.5 μM N-Srv2 +/− 0.5 μM Twf1 was applied to grids and negative stained as above. Images were captured using an FEI Morgani 268 transmission electron microscope at an acceleration voltage of 80 kV and magnifications of 14000, 18000 or 22000. Images are representative from experiments repeated 2–3 times.

F-actin cosedimentation assays

Different concentrations (2, 4, 6, 8 μM) of preformed F-actin were incubated with Twf1, Twf1Δtail, MBP-Twf1 tail, or MBP-Twf1-10 tail for 10 min at room temperature. Reactions were centrifuged at 350,000 × g for 30 min at 20°C. Supernatant and pellet fractions were

analyzed on gels by Coomassie staining and quantified by scanning densitometry. Each Twf1 construct was processed in parallel reactions lacking F-actin, and the fraction of Twf1 that pelleted non-specifically was subtracted from the analysis. For MBP-Twf1 tail and MBP-Twf1-10 tail, owing to their molecular weights being very close to that of actin, the relative abundance of protein in the supernatant and pellet fractions was determined by quantitative Western blot using α-MBP antibody (NEB; E8038S) at 1:10,000 dilution.

Fluorescence Anisotropy

100 nM of Oregon Green ATP-G-actin was mixed with various concentrations of wild-type and mutant Twf1 in G-buffer (5 mM Tris pH 7.5, 0.1 mM $CaCl_2$, 0.5 mM DTT and 0.2 mM ATP), and incubated at room temperature for 15 min. Then anisotropy was determined by measuring polarized emission intensities at 530 nm when excited at 488 nm (mean intensity over a 2 min time period). Anisotropy values were normalized against control reactions lacking Twf1.

Supernatant Depletion Assays

GST-N-Srv2 and GST alone (20 μM final) were bound to glutathione agarose beads and mixed for 20 min with 2 μM Twf1 and/or 2 μM ADP-G-actin. Supernatants were collected and analyzed on gels by Coomassie staining. Reactions were carried out in 5 mM Tris-HCl pH 8.0, 100 mM KCl, 0.2 mM $CaCl_2$, 0.4 mM DTT, and 0.2 mM ADP.

Plasmid Shuffle Assays

A *twf1*Δ *cof1-22* mutant yeast strain carrying a *URA3*-marked wild-type *TWF1* plasmid (pRS316-Twf1) to maintain viability was transformed with the following *HIS3*-marked plasmids: pRS313 (empty vector), pRS313-Twf1, pRS313-Twf1-9N, pRS313-Twf1-9C, and pRS313-Twf1-99. Cells were grown to saturation in His- media, plated as serial dilutions on Ura- or 5-fluoroorotic acid (5-FOA) media, and grown at 25°C for 3 days.

Quantitative immunoblotting to determine cellular levels of proteins

Whole cell extracts (WCEs) were prepared from a wild-type yeast strain (BGY12) grown in rich medium (YPD) to an OD_{600} = 1 as described. Total protein concentration in WCEs was determined using a Coomassie spot assay and a BSA standard curve. For each protein quantified (actin, Srv2, and Twf1), three different amounts of WCE were immunoblotted in parallel with known quantities of the purified proteins. Antibodies raised in hens (Aves Inc., Tigard, OR) against yeast actin and Srv2, and in rabbits against yeast Twf1 [20] were used at dilutions of 1:20,000, 1:7000, and 1:1000, respectively. HRP-conjugated secondary antibodies, anti-chicken (Aves, Inc.) or anti-rabbit (GE Healthcare), were used at 1:10,000. Signals were detected by chemiluminescence and quantified by densitometry. Bands with intensities in the linear range of the standard curve were used to calculate ng of the specific protein per μg of total cellular protein. Molar concentrations of these proteins in WCEs were calculated from their cellular abundance (ng/μg total protein), molecular weights, and the concentration of total protein in the extract (4.2μg/μl). These values were used to calculate cellular concentrations by measuring cell densities (using a haemocytometer) in the samples used to make WCEs. Based on electron micrographs of yeast cells, we estimated that over

half of the cell volume is occupied by non-cytosolic compartments (e.g. cell wall, vacuole, mitochondria, plasma membrane, endoplasmic reticulum, and Golgi). Thus, we make a conservative estimate that the cytosolic concentrations of these proteins are two fold higher than their calculated cellular concentrations.

Statistical Analysis

All experiments were repeated at least twice, as indicated in the legends and elsewhere in the methods. Representative rather than aggregated data sets are presented where indicated. Averages and SD (Fig 1B) or SEM (all other error bars) and detailed n values for each figure panel are stated in the corresponding legends. A two-tailed student's t-test (for comparisons between two conditions) or one-way ANOVA analysis (for comparisons between multiple conditions) was used for statistical analysis. No statistical method was used to predetermine sample size.

Supplementary Material

Refer to Web version on PubMed Central for supplementary material.

Acknowledgments

We are extremely grateful to Dennis Breitsprecher, Melissa Cataldo, Zvonimir Dogic, Julian Eskin, Silvia Jansen, James Moseley, and Avital Rodal for helpful comments on the manuscript. We thank Anya Goodman for extensive help with the cellular concentration experiments. This work was supported by grants from NIH (GM063691) and National Science Foundation (DMR-MRSEC-0820429) to B.L.G.

References

1. Campellone KG, Welch MD. A nucleator arms race: cellular control of actin assembly. Nat Rev Mol Cell Biol. 2010; 11(4):237–251. [PubMed: 20237478]
2. Brieher W. Mechanisms of actin disassembly. Mol Biol Cell. 2013; 24(15):2299–2302. [PubMed: 23900650]
3. Pollard TD. Rate constants for the reactions of ATP- and ADP-actin with the ends of actin filaments. J Cell Biol. 1986; 103(6):2747–2754. [PubMed: 3793756]
4. Kuhn JR, Pollard TD. Real-time measurements of actin filament polymerization by total internal reflection microscopy. Biophys J. 2005; 88(2):1387–1402. [PubMed: 15556992]
5. Watanabe N, Mitchison TJ. Single-molecule speckle analysis of actin filament turnover in lamellipodia. Science. 2002; 295(5557):1083–1086. [PubMed: 11834838]
6. Miyoshi T, Watanabe N. Can filament treadmilling alone account for the F-actin turnover in lamellipodia? Cytoskeleton. 2013; 70(4):179–190. [PubMed: 23341338]
7. Ono S. Mechanism of depolymerization and severing of actin filaments and its significance in cytoskeletal dynamics. Int Rev Cytol. 2007; 258:1–82. [PubMed: 17338919]
8. Jansen S, et al. Single-molecule imaging of a three-component ordered actin disassembly mechanism. Nat Commun. 2015; 6(7202)
9. Poukkula M, Kremneva E, Serlachius M, Lappalainen P. Actin-depolymerizing factor homology domain: a conserved fold performing diverse roles in cytoskeletal dynamics. Cytoskeleton. 2011; 68(9):471–490. [PubMed: 21850706]
10. Ono S. The role of cyclase-associated protein in regulating actin filament dynamics – more than a monomer-sequestration factor. J Cell Sci. 2013; 126(Pt 15):3249–3258. [PubMed: 23908377]
11. Goode BL, Drubin DG, Lappalainen P. Regulation of the cortical actin cytoskeleton in budding yeast by twinfilin, a ubiquitous actin monomer-sequestering protein. J Cell Biol. 1998; 142(3): 723–733. [PubMed: 9700161]

12. Vartiainen M, Ojala PJ, Auvinen P, Peranen J, Lappalainen P. Mouse A6/twinfilin is an actin monomer-binding protein that localizes to regions of rapid actin dynamics. Mol Cell Biol. 2000; 20(5):1772–1783. [PubMed: 10669753]
13. Wahlstrom G, et al. Twinfilin is required for actin-dependent developmental processes in Drosophila. J Cell Biol. 2001; 155(5):787–796. [PubMed: 11724820]
14. Vartiainen MK, Sarkkinen EM, Matilainen T, Salminen M, Lappalainen P. Mammals have two twinfilin isoforms whose subcellular localizations and tissue distributions are differentially regulated. J Biol Chem. 2003; 278(36):34347–34355. [PubMed: 12807912]
15. Iwasa JH, Mullins RD. Spatial and temporal relationships between actin-filament nucleation, capping, and disassembly. Curr Biol. 2007; 17(5):395–406. [PubMed: 17331727]
16. Peng AW, Belyantseva IA, Hsu PD, Friedman TB, Heller S. Twinfilin 2 regulates actin filament lengths in cochlear stereocilia. J Neurosci. 2009; 29(48):15083–15088. [PubMed: 19955359]
17. Rzadzinska AK, Nevalainen EM, Prosser HM, Lappalainen P, Steel KP. MyosinVIIa interacts with Twinfilin-2 at the tips of mechanosensory stereocilia in the inner ear. PLoS One. 2009; 4(9):e7097. [PubMed: 19774077]
18. Helfer E, et al. Mammalian twinfilin sequesters ADP-G-actin and caps filament barbed ends: implications in motility. EMBO J. 2006; 25(6):1184–1195. [PubMed: 16511569]
19. Paavilainen VO, et al. Structural basis and evolutionary origin of actin filament capping by twinfilin. Proc Natl Acad Sci USA. 2007; 104(9):3113–3118. [PubMed: 17360616]
20. Palmgren S, Ojala PJ, Wear MA, Cooper JA, Lappalainen P. Interactions with PIP2, ADP-actin monomers, and capping protein regulate the activity and localization of yeast twinfilin. J Cell Biol. 2001; 155(2):251–260. [PubMed: 11604420]
21. Paavilainen VO, et al. Structural conservation between the actin monomer-binding sites of twinfilin and actin-depolymerizing factor (ADF)/cofilin. J Biol Chem. 2002; 277(45):43089–43095. [PubMed: 12207032]
22. Normoyle KP, Brieher WM. Cyclase-associated protein (CAP) acts directly on F-actin to accelerate cofilin-mediated actin severing across the range of physiological pH. J Biol Chem. 2012; 287(42):35722–35732. [PubMed: 22904322]
23. Chaudhry F, et al. Srv2/cyclase-associated protein forms hexameric shurikens that directly catalyze actin filament severing by cofilin. Mol Biol Cell. 2013; 24(1):31–41. [PubMed: 23135996]
24. Jansen S, Collins A, Golden L, Sokolova O, Goode BL. Structure and mechanism of mouse cyclase-associated protein (CAP1) in regulating actin dynamics. J Biol Chem. 2014; 289(44): 30732–30742. [PubMed: 25228691]
25. Quintero-Monzon O, et al. Reconstitution and dissection of the 600-kDa Srv2/CAP complex: roles for oligomerization and cofilin-actin binding in driving actin turnover. J Biol Chem. 2009; 284(16):10923–10934. [PubMed: 19201756]
26. Blanchoin L, Pollard TD. Mechanism of interaction of *Acanthamoeba actophorin* (ADF/Cofilin) with actin filaments. J Biol Chem. 1999; 274(22):15538–15546. [PubMed: 10336448]
27. McGough A, Pope B, Chiu W, Weeds A. Cofilin changes the twist of F-actin: implications for actin filament dynamics and cellular function. J Cell Biol. 1997; 138(4):771–781. [PubMed: 9265645]
28. Tarassov K, et al. An in vivo map of the yeast protein interactome. Science. 2008; 320(5882): 1465–1470. [PubMed: 18467557]
29. Breitkreutz A, et al. A global protein kinase and phosphatase interaction network in yeast. Science. 2010; 328(5981):1043–1046. [PubMed: 20489023]
30. Okada K, Obinata T, Abe H. XAIP1: a *Xenopus* homologue of yeast actin interacting protein 1 (AIP1), which induces disassembly of actin filaments cooperatively with ADF/cofilin family proteins. J Cell Sci. 1999; 112(10):1553–1565. [PubMed: 10212149]
31. Falck S, et al. Biological role and structural mechanism of twinfilin-capping protein interaction. EMBO J. 2004; 23(15):3010–3019. [PubMed: 15282541]
32. Mattila PK, et al. A high-affinity interaction with ADP-actin monomers underlies the mechanism and in vivo function of Srv2/cyclase-associated protein. Mol Biol Cell. 2004; 15(11):5158–5171. [PubMed: 15356265]

33. Chaudhry F, et al. Autonomous and in trans functions for the two halves of Srv2/CAP in promoting actin turnover. Cytoskeleton. 2014; 71(6):351–360. [PubMed: 24616256]

34. Moseley JB, et al. A conserved mechanism for Bni1- and mDia1-induced actin assembly and dual regulation of Bni1 by Bud6 and profilin. Mol Biol Cell. 2004; 15(2):896–907. [PubMed: 14657240]

35. Spudich JA, Watt S. The regulation of rabbit skeletal muscle contraction. I. Biochemical studies of the interaction of the tropomyosin-troponin complex with actin and the proteolytic fragments of myosin. J Biol Chem. 1971; 246(15):4866–4871. [PubMed: 4254541]

36. Breitsprecher D, et al. Rocket launcher mechanism of collaborative actin assembly defined by single molecule imaging. Science. 2013; 336(6085):1164–1168. [PubMed: 22654058]

37. Pollard TD, Cooper JA. Quantitative analysis of the effect of *Acanthamoeba* profilin on actin filament nucleation and elongation. Biochemistry. 1984; 23(26):6631–6641. [PubMed: 6543322]

38. Carlier MF, Pantaloni D. Direct evidence of ADP-Pi-F-actin as the major intermediate in ATP-actin polymerization. Rate of dissociation of Pi from actin filaments. Biochemistry. 1986; 25(24): 7789–7792. [PubMed: 3801442]

39. Blanchoin L, Pollard TD. Hydrolysis of ATP by polymerized actin depends on the bound divalent cation but not profilin. Biochemistry. 2002; 41(2):597–602. [PubMed: 11781099]

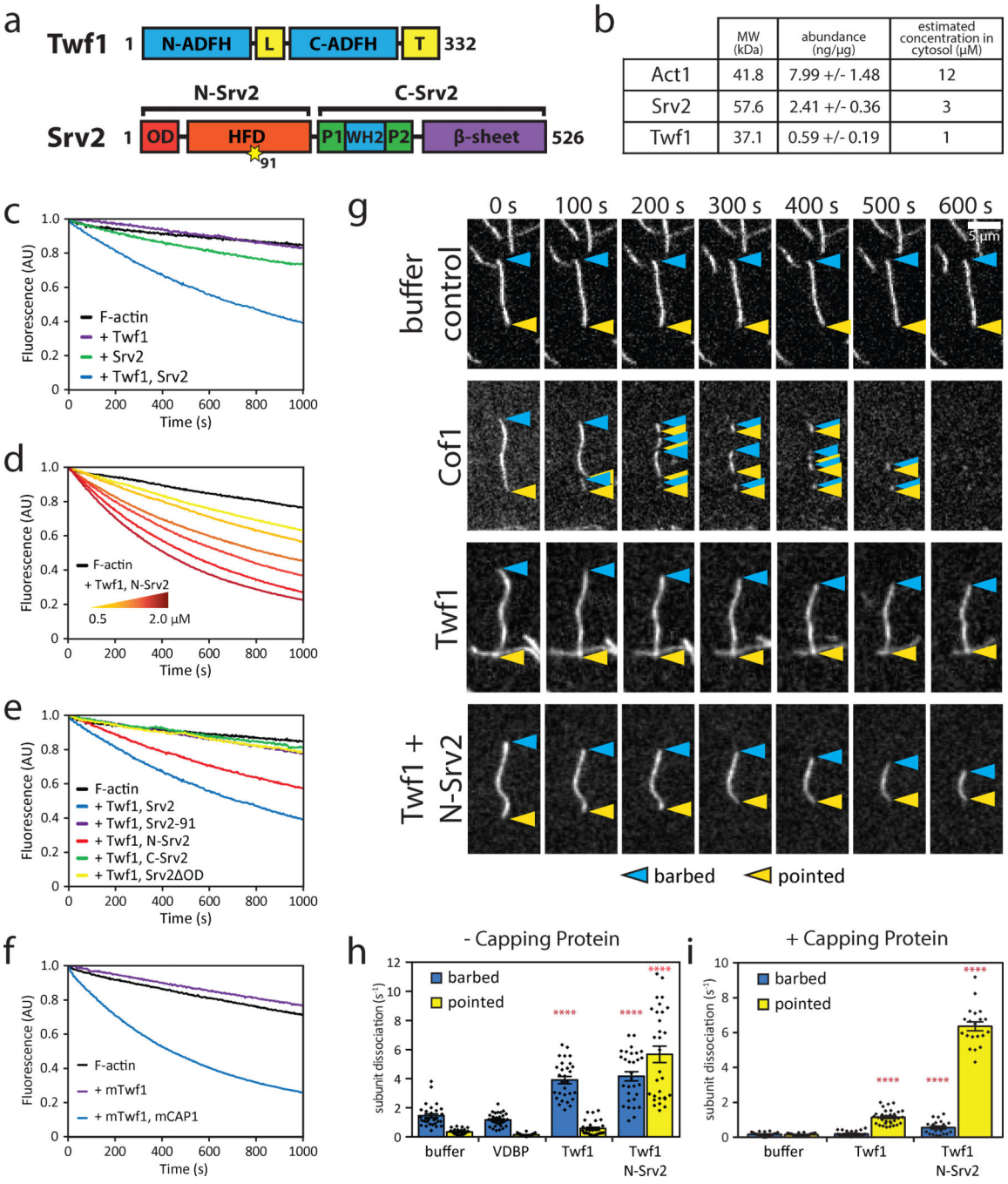

Fig. 1.

Twinfilin and Srv2 accelerate depolymerization from actin filament ends. **(A)** Twf1 and Srv2/CAP domain organization: ADFH, actin depolymerization factor homology domain; L, linker; T, tail; OD, oligomerization domain; HFD, helical folded domain; P1 and P2, polyproline tracts. **(B)** Cytosolic concentrations of Actin, Srv2, and Twf1 measured by quantitative immunoblotting. Protein abundance expressed in ng/µg total cellular protein (+/− SD) was measured from n = 11, 5, and 8 independent experiments for Actin, Srv2, and Twf1, respectively. **(C–F)** Bulk F-actin depolymerization assays induced by Vitamin-D

Binding Protein. Reactions: 2 μM F-actin (10% pyrene-labeled), 100 nM yeast Capping Protein, 1 μM yeast Twf1 (or mouse mTwf1), 1 μM yeast Srv2 (or mouse mCAP1) constructs, except in D, where different concentrations and ratios of Twf1 and N-Srv2 were used (yellow to red gradient: 0.5/0.5, 0.5/1.0, 1.0/1.0, 1.0/2.0, 1.5/2.0, 2.0/2.0 μM Twf1/N-Srv2). Data are representative examples of experiments repeated 2–3 times each. **(G)** Representative time lapse TIRF microscopy of tethered actin filaments (10% OG-labeled, 0.5% biotin-actin) disassembling in the presence or absence of 10 nM Cof1, 0.5 μM Twf1, and/or 0.5 μM N-Srv2. Blue arrows, barbed ends; yellow arrows, pointed ends. **(H, I)** Filament depolymerization rates (subunits s^{-1}) in the absence (H) or presence (I) of Capping Protein, measured from TIRF reactions as in (G). For (H), rates for each condition (left to right) were pooled from two independent experiments (n = 29, 32, 29, 30 filaments), giving mean depolymerization rates of 1.455, 1.174, 3.911, and 4.171 subunits s^{-1} at the barbed end, and 0.341, 0.152, 0.583, and 5.676 subunits s^{-1} at the pointed end. For (I), rates from each condition (left to right) were pooled from 2, 1 and 1 independent experiments, respectively (n = 22, 31, 20 filaments), giving mean depolymerization rates of 0.171, 0.197, and 0.562 subunits/s at the barbed end, and 0.150, 1.148, and 6.361 subunits/s at the pointed end. Error bars, SEM. ****$p \leq 0.0001$, one-way ANOVA with Tukey post-hoc test. Statistics source data can be found in Supplementary Table 1.

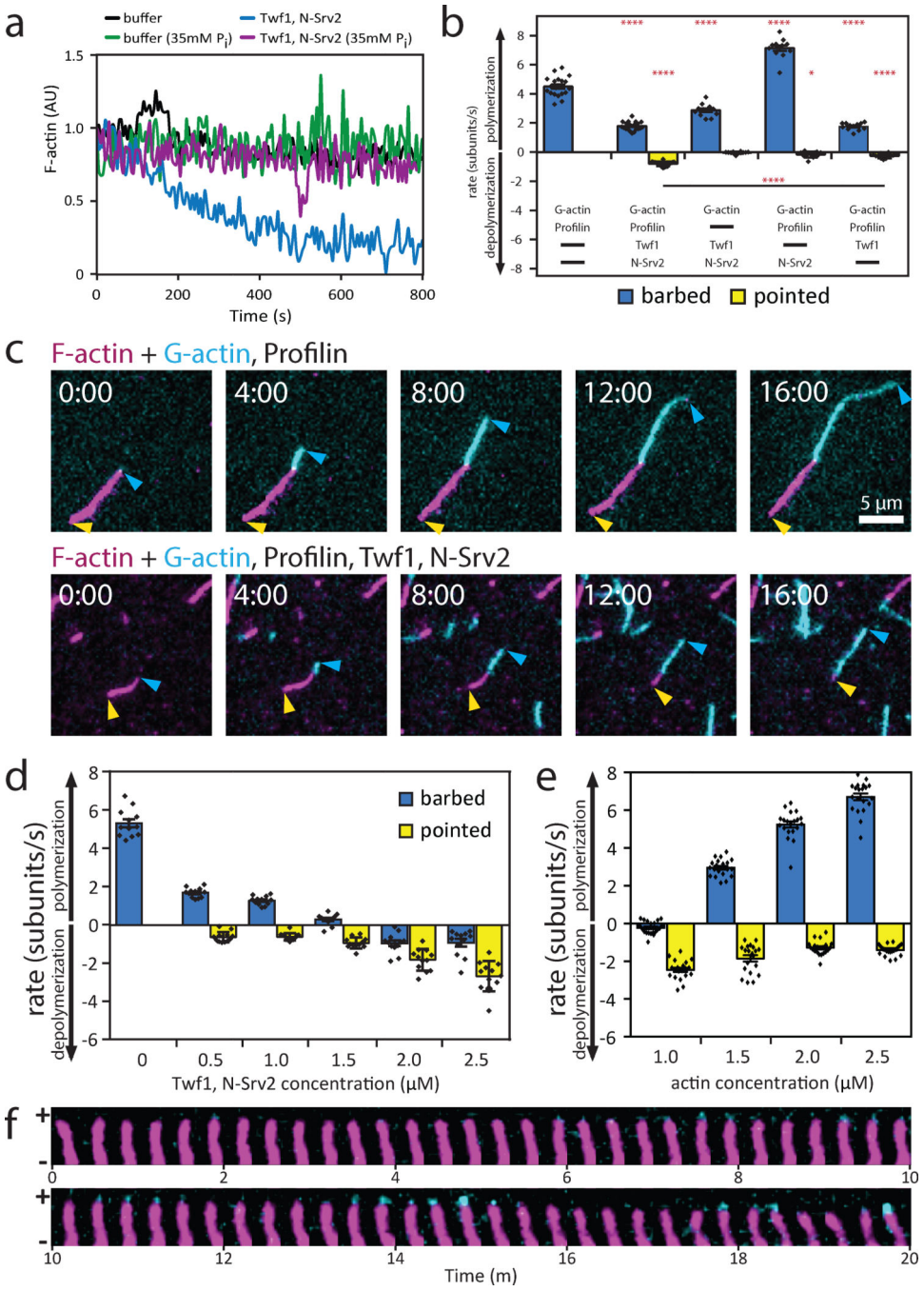

Fig. 2.

Reconstitution and direct visualization of actin filament treadmilling under assembly-promoting conditions. **(A)** Total F-actin fluorescence signal over time in TIRF reactions of tethered filaments (10% OG-labeled, 0.5% biotin-actin) disassembling in the presence or absence of 0.5 µM Twf1 and 0.5 µM N-Srv2, in the additional presence or absence of 35 mM free P_i, which drives filaments into the ADP+P_i state. Data are average curves from two fields of view from one representative experiment, repeated twice. **(B)** Different combinations of 1 µM G-actin (10% OG-labeled, 0.5% biotin-actin), 5 µM Profilin, 1 µM

Twf1, and 1 μM N-Srv2, as indicated, were added to preassembled DY647-actin filaments (5% DY647-labeled, 0.5% biotin-actin). Graph shows average rates of elongation/depolymerization at each end. Rates for each condition (left to right) were measured from 1 representative experiment (n = 20, 20, 12, 12, 12 filaments, respectively). Barbed end rates: 4.500, 1.785, 2.876, 7.140, and 1.767 subunits s^{-1}; pointed end rates: 0, −0.804, −0.039, −0.158, −0.264 subunits s^{-1}, respectively. Error bars, SEM. Significance measured against control G-actin + Profilin reactions, except where indicated; ****$p \leq 0.0001$, *$p \leq 0.05$, one-way ANOVA with Tukey post-hoc test. **(C)** Direct visualization of F-actin treadmilling in TIRF reactions. 5 μM Profilin, 1 μM G-actin (10% OG-labeled, 0.5% biotin-actin, cyan), and 0.5 μM each of Twf1 and N-Srv2 were added to preassembled DY647-actin (5% DY647-labeled, 0.5% biotin-actin, magenta) filaments. Blue arrows, barbed ends; yellow arrows, pointed ends. **(D, E)** Rates of elongation and/or depolymerization at each filament end, in (D) with a fixed concentration of G-actin (1.0 μM) and the indicated concentrations of Twf1 and N-Srv2, and in (E) with a fixed concentration of Twf1/N-Srv2 (2.0 μM each) and the indicated concentrations of G-actin. For (D), rates were from 1 representative experiment (n = 12 filaments per condition). Barbed end rates: 5.349, 1.703, 1.291, 0.293, −0.950, and −0.918 subunits/s; pointed end rates: 0, −0.628, −0.611, −0.937, −1.814, and −2.675 subunits/s, respectively. R^2 = 0.808 barbed end, R^2 = 0.739 pointed end. For (E), rates were from 1 representative experiment (n = 20 filaments per condition). Barbed end rates: −0.229, 2.951, 5.243, and 6.703 subunits s^{-1}; pointed end rates: −2.454, −1.849, −1.286, and −1.411 subunits/s, respectively. R^2 = 0.924 barbed end, R^2 = 0.373 pointed end. Error bars, SEM. $p < 0.0001$, one-way ANOVA with post-hoc test for linear trend. **(F)** Time lapse TIRF imaging of alternating runs of polymerization (cyan) and depolymerization at the barbed end of a single filament, in the presence of 1.5 μM Twf1, 1.5 μM N-Srv2, 5 μM Profilin, and 1 μM G-actin. Images are representative of reactions repeated 3 times. Statistics source data for (B, D, E) in Supplementary Table 1.

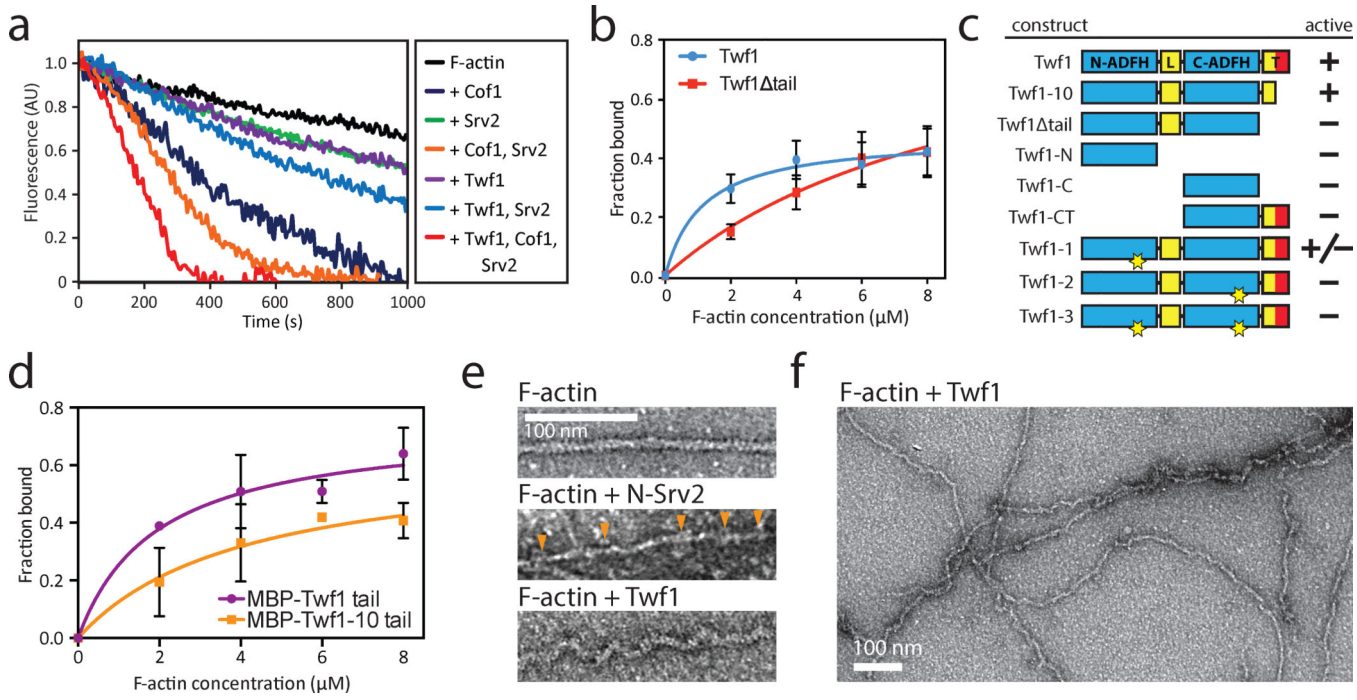

Fig. 3.

Mechanism and domain requirements for Twinfilin depolymerization activity. **(A)** Total F-actin fluorescence signal over time of tethered filaments (10% OG-labeled, 0.5% biotin-actin) disassembling in TIRF reactions containing 100 nM Capping Protein, and 10 nM Cof1, 0.5 μM Twf1, 0.5 μM Srv2, as indicated. Data are average curves from two fields of view from a single representative experiment, which was repeated twice. **(B)** Quantification of the fraction of Twf1 or Twf1Δtail (2 μM) that cosediments with increasing concentrations of F-actin. Curves fit by non-linear regression. Error bars, SEM (n = 3 experiments per condition). Statistics source data can be found in Supplementary Table 1. **(C)** Activities of indicated Twf1 constructs (1 μM) in bulk F-actin disassembly assays containing 100 nM Capping Protein and 1 μM N-Srv2 (see Supplemental Fig. 1B,C). Twf1-1 and Twf1-2 carry mutations in the N- and C-terminal ADFH domain 'G/F sites', respectively; Twf1-3 carries mutations in both sites [20]. **(D)** Quantification of fraction of MBP-Twf1 tail (305-332) or MBP-Twf1-10 tail (305-322) (2 μM) that cosediments with increasing concentrations of F-actin. Curves fit by non-linear regression. Error bars, SEM (n = 3 experiments per condition). Statistics source data can be found in Supplementary Table 1. **(E)** Electron micrographs of actin filaments, alone and decorated with N-Srv2 or Twf1. Orange arrows indicate extra densities on filament sides corresponding to N-Srv2 hexamers. **(F)** Wider field electron micrographs of actin filaments decorated with Twf1. EM images are representative from experiments repeated 2–3 times.

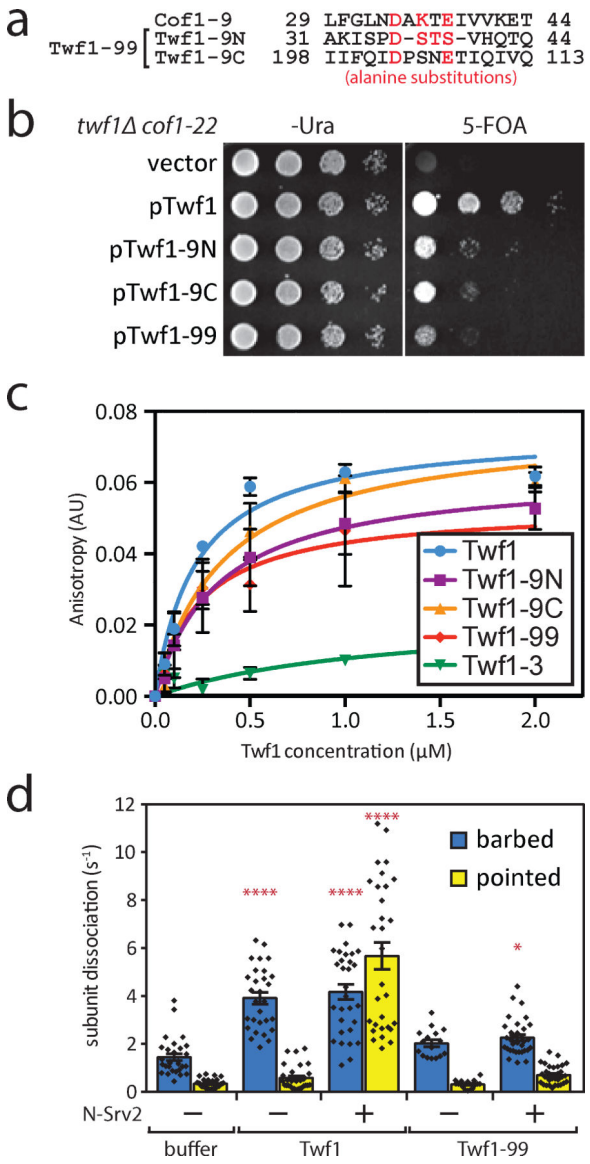

Fig. 4.

The depolymerization activity of Twinfilin is important for its cellular function. **(A)** Design of mutations analogous to Cof1-9 introduced into Twf1's N-terminal ADFH domain (Twf1-9N) and C-terminal ADFH domain (Twf1-9C). Twf1-99 carries both the 9N and 9C mutations. **(B)** Serial dilutions of *twf1Δ cof1-22* yeast cells, carrying a *URA3*-marked *TWF1* plasmid to maintain viability, transformed with the indicated *HIS3*-marked plasmids and grown on Ura^- or anti-selective 5-FOA media. Data shown are representative examples of experiments repeated 3 times each. **(C)** Fluorescence anisotropy measurements of OG-labeled G-actin incubated in the presence of increasing concentrations of the indicated Twf1 constructs. Curves fit by non-linear regression. Error bars, SEM (n = 3 experiments per condition). Statistics source data can be found in Supplementary Table 1. **(D)** Filament depolymerization rates (subunits s^{-1}) of the indicated Twf1 constructs in the absence or presence of N-Srv2 measured in TIRF reactions.. Rates for each condition (left to right)

were pooled from 1–2 independent experiments (n = 29, 29, 30, 16, and 33 filaments), giving mean depolymerization rates of 1.455, 3.911, 4.171, 2.029, and 2.268 subunits/s at the barbed end, and 0.341, 0.583, 5.676, 0.318, and 0.706 subunits/s at the pointed end. Error bars, SEM. ****$p < 0.0001$ for barbed end rate of Twf1 + N-Srv2 versus buffer or Twf1. **** $p < 0.0001$ for pointed end rates of Twf1 and Twf1 + N-Srv2 versus buffer. * $p < 0.05$ for barbed end rate of Twf1-99 + N-Srv2 versus buffer. All other pairings, ns. One-way ANOVA with Tukey post-hoc test. Statistics source data can be found in Supplementary Table 1.

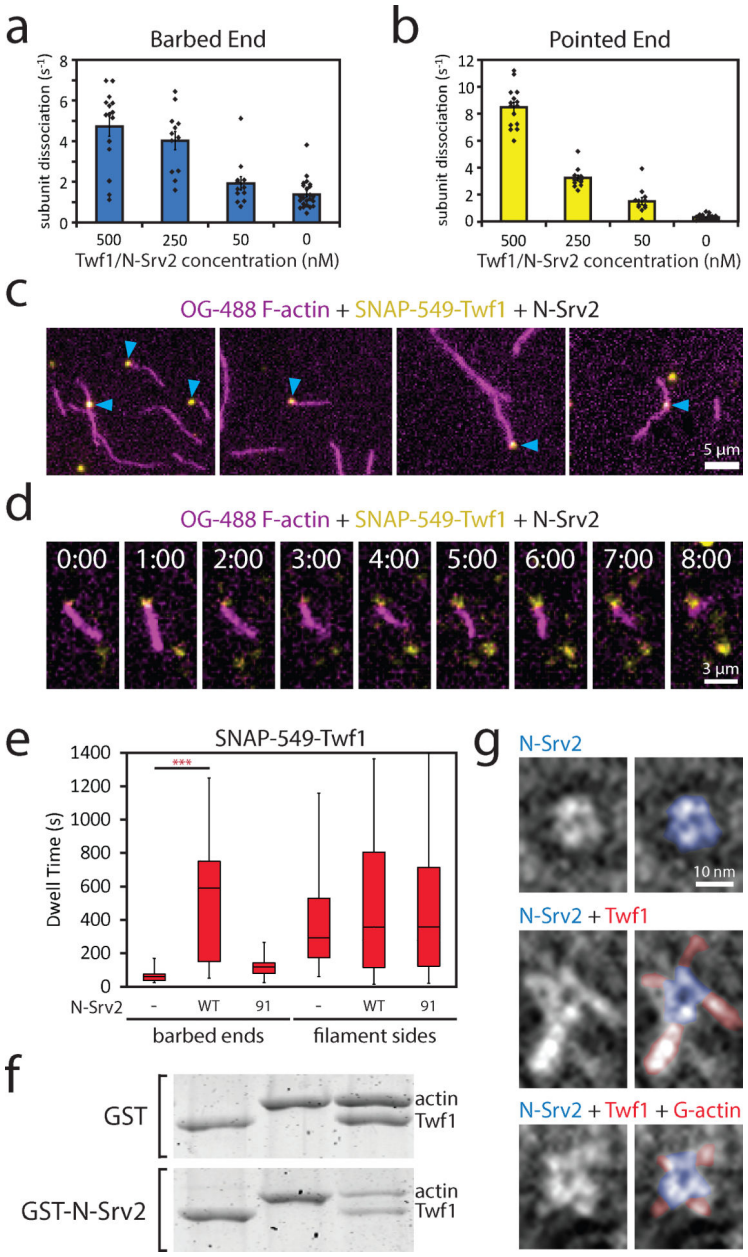

Fig. 5.

Twinfilin interactions with F-actin and N-Srv2 visualized by multi-wavelength TIRF and electron microscopy. **(A, B)** Rates of depolymerization (subunits s^{-1}) at the barbed (A) and pointed (B) ends of the same filaments (10% OG-labeled, 0.5% biotin-actin), in the presence of variable concentrations of Twf1 and N-Srv2 (equimolar) as indicated. Rates for each concentration (left to right) measured from 1 representative experiment (n = 15, 12, 12, 24 filaments), giving mean depolymerization rates of 4.730, 4.022, 1.927, and 1.369 subunits/s at the barbed end, and 8.485, 3.236, 1.522, and 0.327 subunits s^{-1} at the pointed end. Error bars, SEM. $p < 0.0001$, one-way ANOVA analysis with post test for linear trend. $R^2 = 0.552$ barbed end, $R^2 = 0.855$ pointed end. **(C)** Representative images of SNAP-549-Twf1 (yellow) interacting with the sides and barbed ends of actin filaments (magenta) in the

presence of N-Srv2. Blue arrows indicate SNAP-549-Twf1 puncta which interact with filaments. Images representative of localization observed in 10 reactions. **(D)** Time lapse images of dual-color TIRF microscopy showing an actin filament (10% OG-labeled, 0.5% biotin-actin, magenta) undergoing depolymerization with a SNAP-549-Twf1 (yellow) spot processively associated with its barbed end (top). Reaction contained 100 nM SNAP-549-Twf1 and 1 μM N-Srv2. Time stamps in min:s. Images are representative of localization observed in 10 reactions. **(E)** Analysis of dwell times of SNAP-549-Twf1 spots associated with barbed ends or sides of filaments in the absence and presence of N-Srv2 (WT) or N-Srv2-91 (n = 11, 17, 8, 32, 45, and 20 events for the 6 conditions from left to right, from 2–4 independent reactions, resulting in mean dwell times of 68.6, 513.2, 120, 410.3, 489.9, and 502.8 s, respectively). Events were relatively rare due to low concentrations of SNAP-549-Twf1 required for visualization. $p = 0.0002$ for barbed end dwell times in the presence versus absence of N-Srv2. Barbed end dwell times in the presence of N-Srv2-91, ns. Filament side dwell times, ns. Two-tailed Student's t-test. Box extends from the 25th to the 75th percentile, line inside the box is the median, whiskers extend to maxima and minima. **(F)** Supernatant depletion assays measuring binding of Twf1 (2 μM) and/or ADP-G-actin (2 μM) to GST or GST-N-Srv2 beads. Data are representative of experiments repeated 3 times. **(G)** Electron micrographs of N-Srv2 hexamers alone, with Twf1, or with Twf1 and G-actin. Right panels are pseudo-colored (N-Srv2, blue; Twf1/G-actin, red). Images are representative from experiments repeated 2–3 times. Statistics source data for (A, B, E) can be found in Supplementary Table 1.